World Academy of Science, Engineering and Technology
International Journal of Mathematical and Computational Sciences
Vol:13, No:2, 2019

Flood Modeling in Urban Area Using a Well-Balanced Discontinuous Galerkin Scheme on Unstructured Triangular Grids

Rabih Ghostine, Craig Kapfer, Viswanathan Kannan, Ibrahim Hoteit

***Abstract*—**Urban flooding resulting from a sudden release of water due to dam-break or excessive rainfall is a serious threatening environment hazard, which causes loss of human life and large economic losses. Anticipating floods before they occur could minimize human and economic losses through the implementation of appropriate protection, provision, and rescue plans. This work reports on the numerical modelling of flash flood propagation in urban areas after an excessive rainfall event or dam-break. A two-dimensional (2D) depth-averaged shallow water model is used with a refined unstructured grid of triangles for representing the urban area topography. The 2D shallow water equations are solved using a second-order well-balanced discontinuous Galerkin scheme. Theoretical test case and three flood events are described to demonstrate the potential benefits of the scheme: (i) wetting and drying in a parabolic basin (ii) flash flood over a physical model of the urbanized Toce River valley in Italy; (iii) wave propagation on the Reyran river valley in consequence of the Malpasset dam-break in 1959 (France); and (iv) dam-break flood in October 1982 at the town of Sumacarcel (Spain). The capability of the scheme is also verified against alternative models. Computational results compare well with recorded data and show that the scheme is at least as efficient as comparable second-order finite volume schemes, with notable efficiency speedup due to parallelization.

***Keywords*—**Flood modeling, dam-break, shallow water equations, Discontinuous Galerkin scheme, MUSCL scheme.

I. Introduction

THE shallow-water equations (SWEs) present a core foundation for a wide range of applications, including flood prediction [1], dam-break floods [2], [3], coastal floods [4], urban floods [5]-[7], ocean tsunami hazards [8], and hurricane induced storm surges [9], among many others. These applications may involve numerical calculation of very complex flow hydrodynamics such as shock-type flow discontinuities, transcritical flows, wetting and drying over irregular topography. A robust numerical scheme is required in order to produce accurate and stable numerical solutions for these applications.

Most popularly, the Godunov approach has emerged in the Finite Volume (FV) framework, which stores and evolves locally averaged flow data (i.e. depth and velocities) over a mesh element [10]-[13]. Its success owes to approximate Riemann solvers [14], which authentically incorporate water jumps and transitions into the discrete numerical formulation. First-order FV models have been favored and improved for practical applications due to their simplicity, conceptual soundness and locality. The latter property offers convenience to further exploit efficiency speed up algorithms, e.g., local time stepping [15] and adaptive mesh refinement [16] and parallelization [17], aside from the extra theoretical/numerical developments made to properly incorporate source terms and wet/dry fronts [18]-[21].

Second-order Godunov-type flood models have also been devised; most commonly, by means of the MUSCL spatial reconstructions added to the standard FV framework [22]-[26] or the use of the local Discontinuous Galerkin (DG) method [27]-[37], which further exploits properties of the finite element method [38]. The MUSCL approach achieves linear polynomial estimates by further involving non-local piecewise-constant data. This non-locality dictates (extrinsic) widening of the calculation stencil, and may therefore have knock on effects on parallel scalability, among other concerns [21], [39]. The (DG) approach is conceptually similar to the original Godunov FV formulation, but enables to get local linear polynomial estimates via a fully conservative translation to the SWEs on the local element level [40], [41]. It has therefore become a powerful alternative for solving the SWE with high parallel scalability, in addition to offering other advantages such as the construction of high-order schemes on adaptive and/or hybrid meshes [42], [35]. Its major drawback in comparison with MUSCL approach, on a given mesh, is the larger number of degrees of freedom, which consequently entails greater computational costs (estimated to be at least 5 times more expensive [7]. The MUSCL and DG approaches have been mostly coupled with an explicit (local) Runge-Kutta (RK) time integration to construct second-order numerical flood models. Within the scope of flood modeling, it is still of practical benefit to compare between the RKDG and the MUSCL approaches pertaining to (i) their response to mesh coarsening and (ii) their response to parallelization, which is the focus of this article.

In line with issue (i), [7] compared RKDG and MUSCL shallow water solvers with application to flood modeling. Their finding reveals that the extra cost and complexity of the RKDG2 model pays off by providing higher-quality predictions on very coarse meshes. However, this study only considered quadrilateral meshes (along with a modal DG basis) and overlooked the aforementioned issue (ii). While results by [35] show that DG-based models on

V. Kannan is with the Department of Mathematics, Kuwait College of Science and Technology, Kuwait.

R. Ghostine is with the Department of Mathematics, Kuwait College of Science and Technology, Kuwait (e-mail: r.ghostine@kcst.edu.kw).

C. Kapfer and I. Hoteit are with King Abdullah University of Science and Technology, Saudi Arabia.

quadrilateral meshes are more efficient and accurate, they remain questionable given the academic nature of the tests on which the comparisons were performed. Reference [43] conducted more realistic comparisons of the trade-offs of mesh-types for a 2D FV Godunov-type flood model. Their work retrieved the above-mentioned conclusion in [35], i.e. on the appeal of quadrilateral meshes, for academic tests; but more realistic testing indicate that each element type (i.e., triangles vs. quadrilaterals) is advantageous under different circumstances. Practically speaking, an unstructured triangular mesh is very appealing to generate and tailor the mesh to the unique geometry of application sites and the ability to locally refine the mesh around areas of interest [44]-[46]. Within this setting, greater operating costs are expected to track the neighboring of data surrounding each cell, and the computation of the MUSCL gradients is more demanding [47].

This work therefore aims to compare nodal RKDG and MUSCL flood model formulations on unstructured triangular meshes, in light of the above-identified issues (i) and (ii). Both formulations are implemented with the same time integration scheme, same slope limiter function and same approaches to incorporating the practical shallow water features. Differences between them are also discussed in terms of level of numerical complexity. The RKDG and MUSCL flood models are jointly assessed for reproducing analytic solutions, experimental and real-scale violent flooding scenarios. Finally, the findings are discussed, summarized and key conclusions are outlined.

II. Governing Equation

The two–dimensional shallow water equations can be written in a conservative form as:

$$\frac{\partial U}{\partial t}+\frac{\partial E\left(U\right)}{\partial x}+\frac{\partial G\left(U\right)}{\partial y}=S(U), \tag{1}$$

or equivalently:

$$\frac{\partial U}{\partial t}+\nabla\cdot F\left(U\right)=S(U), \tag{2}$$

where, t is the time, x and y are the Cartesian coordiantes, U and $F\left(U\right)=\left(E\left(U\right),G\left(U\right)\right)$ denote the vectors of conserved flow variables and the flux, and S is the source vector. Neglecting Coriolis effects, kinetic and turbulence viscous terms and wind stresses, S only includes bed slope source S_0 and friction source S_f. These vectors are expressed as

$$U=\begin{pmatrix} h \\ q_x \\ q_y \end{pmatrix}, E=\begin{pmatrix} q_x \\ uq_x+gh^2/2 \\ uq_y \end{pmatrix}, G=\begin{pmatrix} q_y \\ vq_x \\ vq_y+gh^2/2 \end{pmatrix}, \tag{3}$$

and

$$S=S_0+S_f=\begin{pmatrix} 0 \\ -gh\frac{\partial z}{\partial x} \\ -gh\frac{\partial z}{\partial y}, \end{pmatrix}+\begin{pmatrix} 0 \\ -gh\frac{n^2u\sqrt{u^2+v^2}}{h^{4/3}} \\ -gh\frac{n^2v\sqrt{u^2+v^2}}{h^{4/3}} \end{pmatrix}, \tag{4}$$

where h is the water depth, u and v are the velocities and q_x and q_y are the unit-width discharges in x- and y-directions (q_x equals to hu and q_y equals to hv), respectively, g is the gravitational acceleration, z is the bottom elevation, and n is the Manning roughness coefficient.

III. RKDG Discretization

The 2D domain Ω is discretised into a mesh of non-overlapping triangles. Multiply (2) by a test function $v\in H^1\left(\Omega_i\right)$ and integrate over the element Ω_i, and use the divergence theorem to obtain the weak formulation

$$\frac{\partial}{\partial t}\int_{\Omega_i}vUd\Omega_i+\int_{\Omega_i}\nabla v\cdot F(U)d\Omega_i-\int_{\partial\Omega_i}vF(U)\cdot n_ids =\int_{\Omega_i}vSd\Omega_i, \tag{5}$$

where n_i is the unit outward facing normal for element Ω_i's edges. To obtain a simpler formulation, we map each element ω_i in the domain to a canonical element Ω_0 with vertices at $(0,0)$, $(1,0)$, and $(0,1)$ with the bijection

$$\begin{pmatrix} x \\ y \\ 1 \end{pmatrix}=\begin{pmatrix} x_1 & x_2 & x_3 \\ y_1 & y_2 & y_3 \\ 1 & 1 & 1 \end{pmatrix}\begin{pmatrix} 1-\xi-\eta \\ \xi \\ \eta \end{pmatrix}, \tag{6}$$

where $\left(x_k,y_k\right),k=1,2,3$, are the vertices of the given triangle, and $(\xi,\eta)\in\Omega_0$. We also map the edges of each element to the canonical interval $I_0=[-1,1]$. This mapping is given by

$$\begin{pmatrix} x \\ y \end{pmatrix}=\begin{pmatrix} x_1 & x_2 \\ y_1 & y_2 \end{pmatrix}\begin{pmatrix} \frac{1}{2}(1-\zeta) \\ \frac{1}{2}(1+\zeta) \end{pmatrix}, \tag{7}$$

where $\left(x_k,y_k\right),k=1,2$, are the endpoints of the given edge and $\zeta\in I_0$.

Let $\Phi=\{\phi_j\}_{j=1}^{N_p}$ be an orthogonal basis of N_p basis functions for $V\left(\Omega_0\right)$ and let U_i over element Ω_i be a linear combination of basis functions ϕ_j

$$U_i=\sum_{j=1}^{N_p}U_{i,j}(t)\phi_j, \tag{8}$$

where $U_{i,j}(t)$ is a vector of solution coefficients. We use an orthonormal basis over Ω_0 and expressed as

$$\begin{aligned}\phi_1&=\sqrt{2},\\ \phi_2&=2-6\xi,\\ \phi_3&=2\sqrt{3}\left(1-\xi-2\eta\right).\end{aligned}$$

Using this orthogonal basis produces a system of ODEs

$$\begin{aligned}\frac{d}{dt}U_{i,j}(t)=&\int_{\Omega_0}F(U_i)\cdot\left(J_i^{-1}\nabla\phi_j\right)d\xi d\eta\\ &-\frac{1}{\det J_i}\sum_{q=1}^{3}\int_{I_0}\phi_jF(U_i)\cdot n_{i,q}l_{i,q}d\zeta\\ &+\int_{\Omega_0}S(U_i)\cdot\phi_jd\xi d\eta,\end{aligned} \tag{9}$$

where $\det J_i$ and $l_{i,q}$ denote the determinants of the Jacobian of (6) and (7), respectively. The surface integrals are discretised using the Gauss three midpoints rule and the boundary integral is approximated by a Gaussian two points rule. The physical fluxes involved in boundary integral are replaced by numerical flux functions based on an approximate Riemann solver [REF Georges] for resolving solving solution discontinuities at the faces between adjacent elements. In

this work, the HLLC Riemann solver [14] is used. Finally, the well-balanced property can be genuinely obtained by projecting the topography function into the same space of local polynomial approximation [48]

$$z_i = \sum_{j=1}^{N_p} z_{i,j}(t)\phi_j, \tag{10}$$

and the partial derivatives of z in the source term S are computed as

$$\frac{\partial z_i}{\partial x} = \sum_{j=1}^{N_p} z_{i,j}(t)\frac{\partial \phi_j}{\partial x} \quad \text{and} \quad \frac{\partial z_i}{\partial y} = \sum_{j=1}^{N_p} z_{i,j}(t)\frac{\partial \phi_j}{\partial y}. \tag{11}$$

A semi-implicit method [49] is applied to evaluate the friction source terms. Finally, each of the local coefficients, $U_{i,j}(j = 1, 2, 3)$ is advanced in time using the explicit double-stage Runge-Kutta time discretization with a CFL number equal to 0.33 [50]. Cockburn and Shus slope limiter [50] is applied to eliminate spurious oscillations around sharp gradients.

IV. Model Validation

In this section, the RKDG model is assessed in relation to its response to i) coarseness to mesh resolution and ii) parallel scalability. The first test case with analytical solution is first used to evaluate the ability of the model to compute flows involving wet/dry front, smooth and sharp flow transitions Then the model is applied to simulate three real flood events and its performance is compared with laboratory and field data as well as with the MUSCL solver.

Parallel simulations are conducted on a 24-core, dual socket 2.5 GHz Intel Xeon Haswell. The parallel implementation platform OpenMP has been used and analyzed in terms of speedup rate and parallel efficiency. The speedup ratio is defined as the execution time of the sequential code divided by the execution time of the parallel code. The parallel efficiency is defined as the speedup divided by the number of threads used. Parallel speedups are measured starting with the serial case, pinning 1 thread per core up to 24 threads.

A. Wetting and Drying in a Parabolic Bowl

The purpose of this test problem is to assess the capacity of the method to capture a moving wet/dry wavefront over irregular topography and nonlinear smooth flow curvatures. Therefore, a nonlinear oscillatory water flow in a parabolic bowl with a moving shoreline is considered. The domain topography follows a parabolic lake defined over $[-4000, 4000]^2$ by

$$z(x, y) = D_0\left(\frac{x^2 + y^2}{L^2} - 1\right). \tag{12}$$

The parameters D_0, L, and Z_0 are constants ($D_0 = 3$ m, $L = 3000$ m, and $Z_0 = 1$ m). The resulting flow will oscillate indefinitely with an amplitude of $w = \left(8gD_0/L^2\right)^{1/2}$ and a period of $T = 2\pi/w$ (i.e., $T = 2457$ s). The analytical solution for the water surface in the frictionless bowl is given by [51]

$$\eta(x, y, t) = D_0\left[\frac{\sqrt{1 - A^2}}{1 - A\cos(wt)} - 1 - \frac{x^2 + y^2}{L^2}\left(\frac{1 - A^2}{(1 - A\cos(wt))^2} - 1\right)\right], \tag{13}$$

$$A = \frac{(D_0 + Z_0)^2 - D_0^2}{(D_0 + Z_0)^2 + D_0^2}. \tag{14}$$

In the numerical simulation, the four boundaries are closed and the initial condition is given by (13), with $t = 0$, $u = v = 0$. The simulation is executed up to one period cycle $T = 2457$ s.

In order to study the response of the RKDG model to a coarsening of spatial resolution, the simulation is run on two different meshes, coarse and fine, consisting of $10,048$ cells and $655,594$ cells, respectively. Figs. 1 and 2 compare the RKDG and MUSCL water level predictions with the analytical solution along the centerline $y = 0$, at $T/4$, $T/2$, $3T/4$, and T (one period cycle is attained). As Figs. 1 and 2 indicate, the coarseness of the mesh seems to have a major impact on the MUSCL predictions of the moving wet/dry shoreline and the flow curvature. However, the MUSCL model provided a much improved prediction of the wet/dry front on the fine mesh (Fig. 2). In contrast, the RKDG model produces excellent predictions on both coarse and fine meshes.

To allow a quantifiable validation, the models are run again on four meshes consisting of $10,048$, $40,886$, $163,840$, and $655,594$ cells, respectively. Errors and associated numerical accuracy orders are presented in Table III. L^2 error is used to reflect the deviation of the numerical results from the analytical solution. For 2D unstructured grids, the area weighted L^2 error has to be used [52], formulated as

$$L^2(U) = \sqrt{\frac{\sum_{i=1}^{n_c} \Omega_i \left(U_i^{Exact} - U_i^{Num.}\right)^2}{\sum_{i=1}^{n_c} \Omega_i}}, \tag{15}$$

where n_c represents the number of cells. Table I lists the L^2 errors and associated orders generated by both MUSCL and RKDG estimation to the water depth at output time T, where Δx represents the average cell length for triangular grids and is computed by $\Delta x = \sqrt{\overline{S}}$ and $\overline{S}$ is the averaged cell area. The results demonstrate that the order of accuracy of the RKDG is higher than that the MUSCL scheme. On average, the order of accuracy of the RKDG scheme is about 1.7 while that of the MUSCL scheme is about 1.3 for this test. As expected, the order of accuracy is predicted to be close to but slightly lower than second-order due to the first-order treatment at the wet-dry front; this is a common numerical phenomenon also reported by many other researchers [31], [19], [12].

In terms of computational cost, the RKDG method is undoubtedly more costly to run than the MUSCL scheme (see Table II). This cost is noted to intensify with increasing level of grid resolution. The average computational time ratio between the two schemes while running in sequence is around 3.07. However, the RKDG model is economical in the sense that it

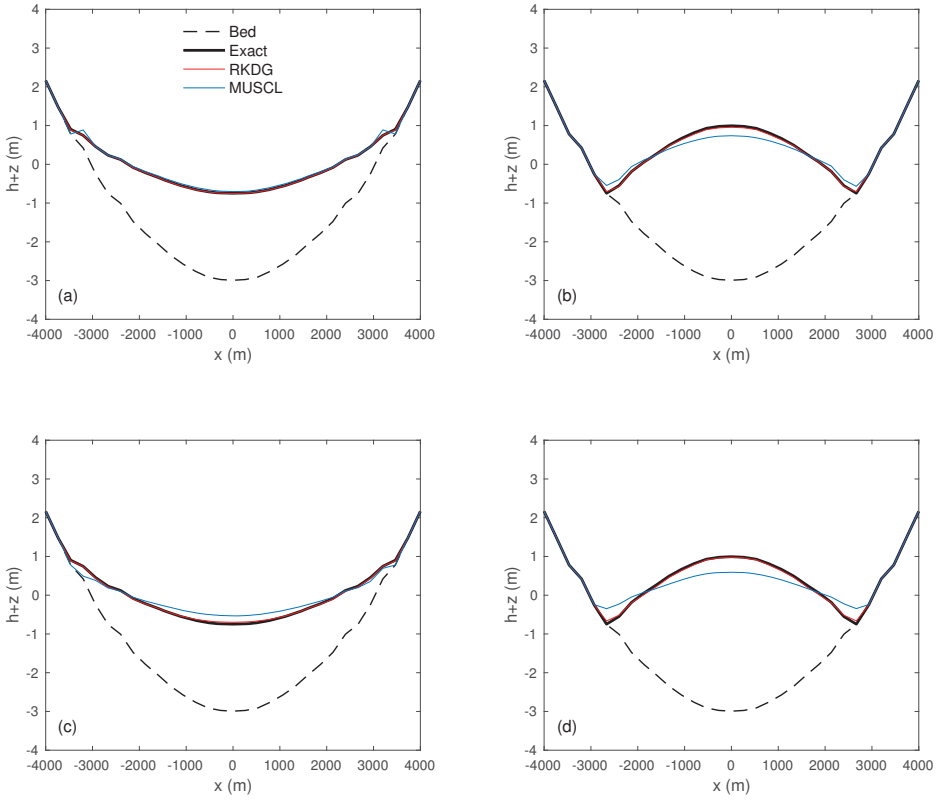

Fig. 1 Wetting and drying in a parabolic bowl: free-surface predictions for the coarse mesh (10,048 triangular cells) (a) $t = T/4$, (b) $t = T/2$, (c) $t = 3T/4$, (d) $t = T$

TABLE I
L^2 ERRORS AND CORRESPONDING ORDERS

	MUSCL		RKDG2	
	L^2-error	L^2-order	L^2-error	L^2-order
Mesh1	9.5E-2	-	8.8E-3	-
Mesh2	4.7E-2	1.0	2.9E-3	1.6
Mesh3	2.1E-2	1.1	9.1E-4	1.6
Mesh4	8.4E-3	1.3	2.8E-4	1.7

provides very reliable simulations on the coarse mesh, while a simulation of equivalent accuracy with the MUSCL scheme requires a finer mesh and, consequently, takes more time to run.

To explore the parallel scalability, the MUSCL and RKDG schemes are run again in parallel. As we can see from Table III, the RKDG scheme provides clearly better speedups than the MUSCL scheme, and despite the RKDG's triple overhead in operational cost. This likely due to the locality in the RKDG formulation to achieve high-order. On the coarse mesh, we observe a speedup rate of 14.89 (62 % parallel efficiency) for the MUSCL scheme and 17.32 (72 % parallel efficiency) for the RKDG scheme. With the fine mesh, better scaling behavior is observed with a speedup rate of 18.95 (79 % parallel efficiency) for the MUSCL scheme and 21.56 (90 % parallel efficiency) for the RKDG scheme. Greater speedup is observed for the fine mesh which is likely due to the increased workload per thread and relative decrease in overhead required to manage the thread pool. The RKDG scheme is around 10 % more efficient in terms of parallel efficiency than the MUSCL scheme on the four meshes. The computational time ratio decreases to 2.66. Taken as whole, the RKDG model appears to be an accurate and reliable alternative for coarse mesh simulation of nonlinear shallow water flow involving cyclic wetting and drying processes.

B. Physical Model of the Toce River Valley

A physical model of a city located within a narrow flood plain was built at ENEL (Milano, Italy) under the EU funded CADAM and IMPACT projects to study extreme flood events [53]. A 5 km reach of the Toce river valley in Italy was scaled down 100 times to reduce the dimensions to 50×13 m in the physical model. Cubic concrete blocks of 0.15 m length were implemented in the upstream reach of the scaled model. In order to separate the effects of the valley topography from those caused solely by the urban district, two masonry walls were placed parallel to the model main axis, thus providing a channelling effect. The Digital Terrain Model (DTM) of the valley are scaled down to a resolution of 0.0025 m^2 covering the 2D domain. Water levels were measured with 0.2 s time step at 10 locations by means of gauges indicated by numbers 1,2,...,10 in Fig. 3.

In the computations, only the 7 m long region located at the upstream end of the physical model was simulated. The numerical grid was composed of 18,400 cells, with an average grid size of 0.03 m. The domain is initially dry and the measured inflow hydrograph is shown in Fig. 4. A free outlet boundary is specified at the downstream end, and the Manning

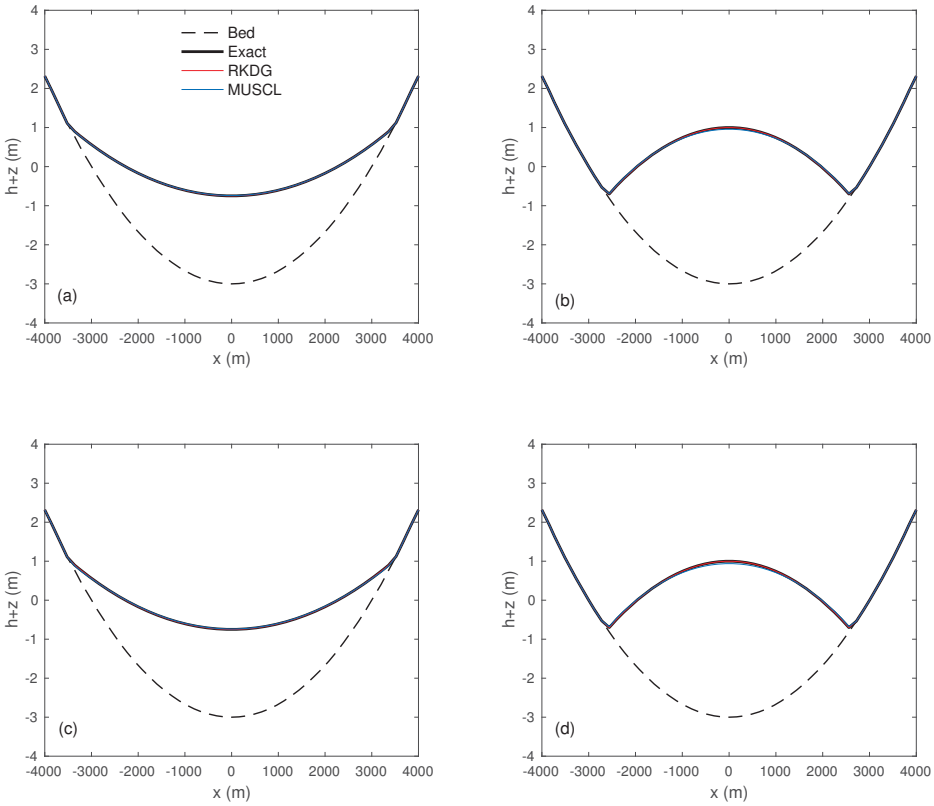

Fig. 2 Wetting and drying in a parabolic bowl: free-surface predictions for the fine mesh (655, 594 triangular cells) (a) $t = T/4$, (b) $t = T/2$, (c) $t = 3T/4$, (d) $t = T$

TABLE II
GENERATED RUNTIME COSTS IN SECOND

	Series			Parallel		
	MUSCL	RKDG2	Ratio	MUSCL	RKDG2	Ratio
Mesh1	35.64	114.77	3.22	2.39	6.63	2.77
Mesh2	206.62	628.75	3.04	12.94	33.39	2.58
Mesh3	2647.13	8179.63	3.09	146.57	398.81	2.72
Mesh4	25733.78	75657.32	2.94	1357.98	3509.15	2.58

TABLE III
SPEEDUP AND PARALLEL EFFICIENCY

	Speedup		Parallel Efficiency (%)	
	MUSCL	RKDG	MUSCL	RKDG
Mesh1	14.89	17.32	62	72
Mesh2	15.97	18.83	67	78
Mesh3	18.06	20.51	75	85
Mesh4	18.95	21.56	79	90

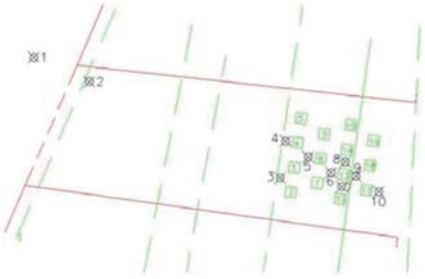

Fig. 3 Physical model of the Toce river valley: locations of the square blocks and gauging stations [53]

coefficient is set to 0.0162 s.m$^{-1/3}$, as recommended by [53].

Fig. 5 shows snapshots of the simulated water surface elevation at $t = 12$ and 20 s. The urban district induced a reduction of the available flow section, which resulted in the formation of strong hydraulic jumps upstream of the buildings and in complex flow features (e.g. wake zones behind the buildings) inside the urban district ($t = 12$ s). As water progressed further downstream into the city, the flow became much more uniform, and the hydraulic jumps propagated in the upstream direction until their intensity decreased with time according to the inflow discharge ($t = 20$ s).

The computed stage-time hydrographs at different gauges are compared with measurements in Fig. 6 as well as with those obtained by MUSCL scheme. The overall trend of stage-time hydrographs was well reproduced although the model tended to underestimate the flow depth at some gauges. The root mean square error RMSE is 0.0075 and 0.01 m for RKDG and MUSCL schemes, respectively.

The RKDG simulations required around $6,107$ s of runtime, while the MUSCL scheme cost $1,651$ s (i.e., roughly 3.7 times less). Next, the two schemes are run in parallel. Quite

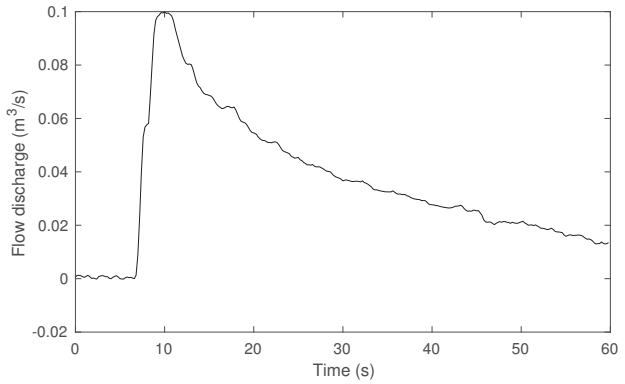

Fig. 4 Physical model of the Toce river valley: inflow hydrograph used as upstream boundary conditions

similar parallel efficiency, as before, is observed with the Toce River test case. The MUSCL scheme achieves a speedup of 16.08 (67% parallel efficiency) and the RKDG scheme achieves a speedup of 19.11 (79% parallel efficiency). The RKDG scheme produces again better scalability results and outperforms the MUSCL scheme by 11%.

C. Malpasset Dam-Break

The Malpasset dam was located in the Reyran river valley in southern France, and collapsed in 1959 after an extremely heavy rain. This disastrous event had already been simulated by [54]-[56], [12] to test their numerical models. Here, it is chosen as a large scale case to verify the current models. The grid consists of $13,541$ nodes and $26,000$ triangular cells and was generated in [54], where the topography data was also provided. As suggested by [54], the real arch dam in simulation is approximated as a straight line between the points of coordinates being (4701.18 m, 4143.41 m) and (4655.50 m, 4392.10 m), and the remnants of the dam after failure are not taken into account. Except for the see and the reservoir where a constant water level of 100 m above see level is assumed, the floodplain is assumed initially dry. The boundaries near the see are set to be transmissive and other ones are regarded as solid walls. Manning coefficient is considered as 0.033 s/m$^{1/3}$ as that in [54]-[56], [12]. The simulation stops when $t = 3600$ s. Fig. 8 illustrates the flood wave evolution by the RKDG model at $t = 1800$ s, when the wave has already reached the downstream floodplain.

A police survey after this accident was undertaken to mark the maximum water levels along the two banks at certain points. The wave arrival times at three electric transformers were also known because the exact times of their shutdowns were recorded. In addition, a physical model with a scale of $1 : 400$ was built and the maximum water levels and the wave propagating processes were measured at 9 gauges along the valley [54]. The locations of the electric transformers, chosen survey points and experimental gauges are sketched in Fig. 3. The results of the survey and the experimental measurements in terms of maximum water levels are compared with the numerical results in Fig. 9.

The numerical results of the model agree well with the survey and measurements, though with some discrepancies, which are perhaps attributed to the limitations of the 2D model in simulating a 3D flow, some measuring uncertainties in survey and experiment, changes of the topography after the event and scale effect in experiment especially for the roughness. As a whole, the RKDG model seems to be at least as accurate as the MUSCL scheme and could obtain approving predictions for such complex flow with wetting and drying over uneven bed on unstructured grid and thus is acceptable for field-scale applications.

The RKDG simulation for this test case lasted around 9395.52 s. In contrast, the MUSCL scheme did the job in 2665.24 s, which is about 3.53 times less. Both schemes are again run in parallel. Once again, the RKDG produces better scalability results yielding a speedup of 17.54 (73 % parallel efficiency). The MUSCL scheme achieves a speedup of 14.96 (62 % parallel efficiency). The computational time ratio is reduced to 3.01. This suggests again that the computational gain obtained using the parallel implementation with the RKDG is more important than the MUSCL scheme.

D. Tous Dam-Break

Tous Dam is the last flood control structure of the Júcar River basin that covers some $21,600$ km^2 of hinterland in the central part of the Mediterranean coast of Spain (Fig. 10). During 20 and 21 October 1982, extremely heavy rainfalls fell over the Tous dam catchment (area of $17,820$ km^2), with an average depth of 500 mm. The total rainfall volume over the basin reached almost 600 million m^3, largely exceeding the storage capacity of the Tous reservoir (120 million m^3). At 19:00 on October 20, the Tous dam failed, giving rise to a flooding wave that reached the cities located downstream of the dam, drastically changing the Júcar valley morphology. The consequences of this event were catastrophic: 300 km^2 of inhabited land were flooded severely; some $200,000$ people were affected and eight casualties were recorded. One of the most affected cities was the small town of Sumacárcel, located about 5 km downstream of the dam. The topography of the town is mountainous and most of the buildings lie on a steep slope terrain, which protected them from the river flow overtopping. However, the older part of the town is located closer to the right bank of a meander of the Júcar river, and was completely flooded on 20 October 1982, with flow depth reaching 67 m at some locations. Two Digital Terrain Models (DTM) with 5 m resolution have been retrieved. The first one dates back to a few weeks after the disaster and the other one was produced in 1998. This case was selected as a benchmark study for the flood propagation workpackage under the EU funded IMPACT project (IMPACT 2004). A complete description of the case study and of the data can be found in [57].

Given the diversity of soils, vegetation coverage, and crop fields present in the area under consideration, it is clear that the roughness varies substantially all over the domain. The areas covered with orange trees appear to have a large influence on the flood propagation, significantly slowing down the flow velocity. These areas located near the town were represented in the numerical computations as areas with a higher friction

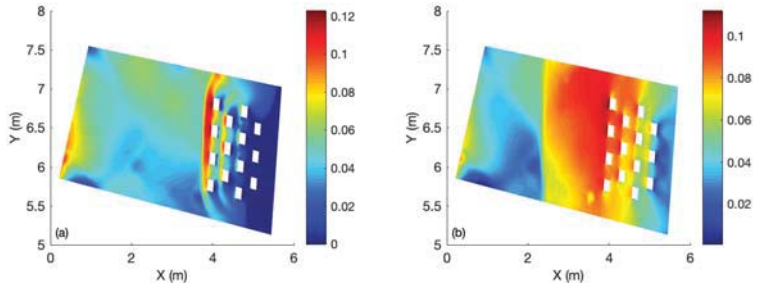

Fig. 5 Physical model of the Toce river valley: computed water level by the RKDG model at (a) $t = 12$ s, (b) $t = 20$ s

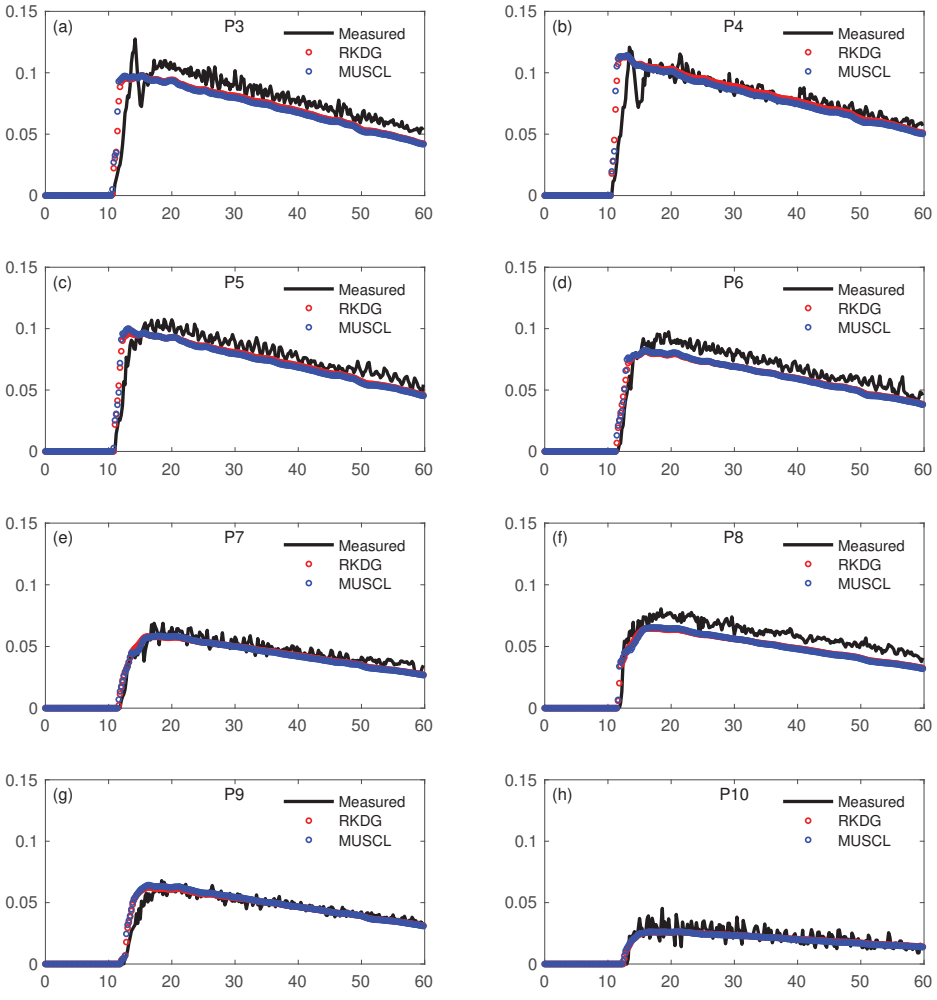

Fig. 6 Physical model of the Toce river valley: computed water level at gauges (a) P3, (b) P4, (c) P5, (d) P6, (e) P7, (f) P8, (g) P9, and (h) P10

coefficient, corresponding to a Manning coefficient of 0.1 s.m$^{-1/3}$. For the rest of the domain, a Manning coefficient of 0.03 s.m$^{-1/3}$ is used, as suggested by [57].

The calculations meshes, the application of the boundary conditions, and also the city model included in the simulations differ between modelers participating in the project [58]-[60]. In this computation, a triangular grid with 25782 cells is used (consistent with the referenced studies). The mesh is finer in the main bed of the river and on the right bank where the city is located. A dry bed condition is initially imposed and the flow discharge hydrograph shown in Fig. 11 is imposed at the upstream boundary condition. For the downstream boundary condition, the flow is assumed critical.

The predicted maximum water depths by the RKDG model are sketched in Fig. 12. Water overflowed the Júcar river banks extensively, flooding the town and reaching depths up to 8 m at some locations. The flood flow path is well predicted along the channel by the two schemes. In addition, reflections and deflections because of irregular boundaries and bed topography are also handled accurately.

Maximum water elevation marks were recorded at 21 locations within, or very close, to Sumacárcel (Fig. 13).

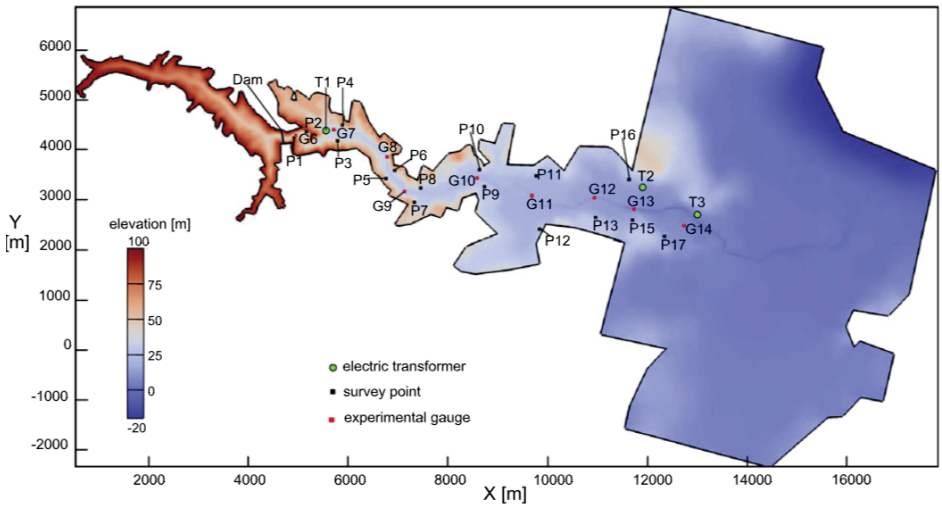

Fig. 7 Malpasset dam-break: Domain with topography and locations of dam, survey points P and experimental gauges G

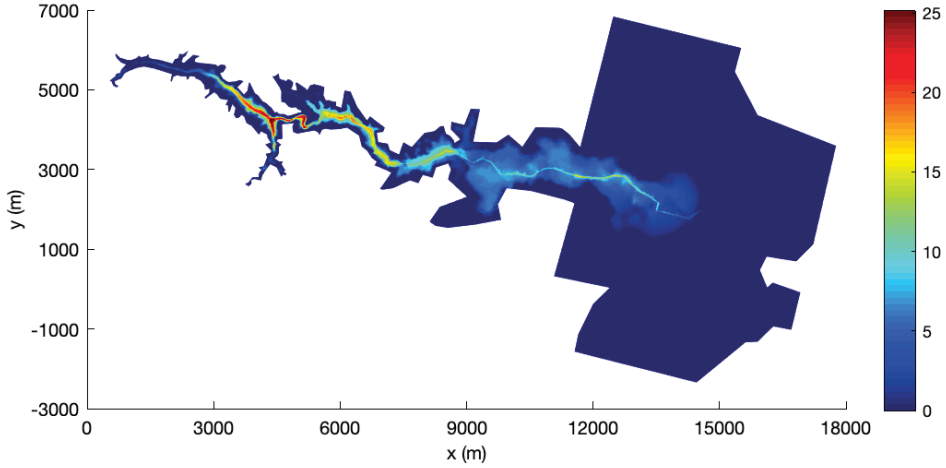

Fig. 8 Malpasset dam-break: numerical flood routing at $t = 1800$ s

The results of the survey and the measurements in terms of maximum water depth are compared with the numerical results in Fig. 14. The numerical results of the RKDG model agree well with the survey and measurements, though with some discrepancies, which could be attributed to the limitations of the 2D models in simulating 3D flows, some uncertainties in survey and measurement, sediment deposition that took place in the river bed just after the dam-break wave, changes of the topography after the event, and scale effect in the experiment especially for the roughness. At gauge 1, the model predicts a lower level than the observed data probably because of its closeness to the upstream boundary of the model, where the inflow condition might include non-negligible uncertainties [61]. This underestimation does not seem to influence the flow immediately upstream, as the model accurately predicts the water depth at gauges 2, 3, 4, 12, 19, and 20. The model is also able to satisfactorily predict the water depth at gauges 5, 6, 7, 8, 9, 10, and 14. However, quite large differences can be observed at gauges 11, 13, 15, 16, and 17. Note that gauges 18 and 21 recorded no flooding (zero flow depth as observed).

The results are are close to those obtained by the MUSCL scheme for this problem. This is probably due to the largeness of the problem domain and the different sources of uncertainties involved, which could affect the accuracy of the schemes. Still, the RKDG scheme performs slightly better than the MUSCL scheme.

The RKDG simulation for this case lasted around 11.36 h. In contrast, the MUSCL scheme did the job in 2.7 h, which is about 4.2 times less than the RKDG scheme. The sequential and parallel codes are also run for the Sumacárcel flooding test. Measured speedups and parallel efficiency are observed to be 20.01 (83%) and 17.13 (71.13%), for the RKDG and MUSCL schemes, respectively. Again, the RKDG consistently performs better and is around 12% more efficient than the MUSCL scheme while running in parallel.

V. Conclusion

Godunov-type numerical solvers to the 2D SWEs on triangular unstructured mesh are of interest to model flood inundation over real and irregular domains. Higher than first-order flood model formulations are beneficial to reduce numerical error over relatively coarse meshes.

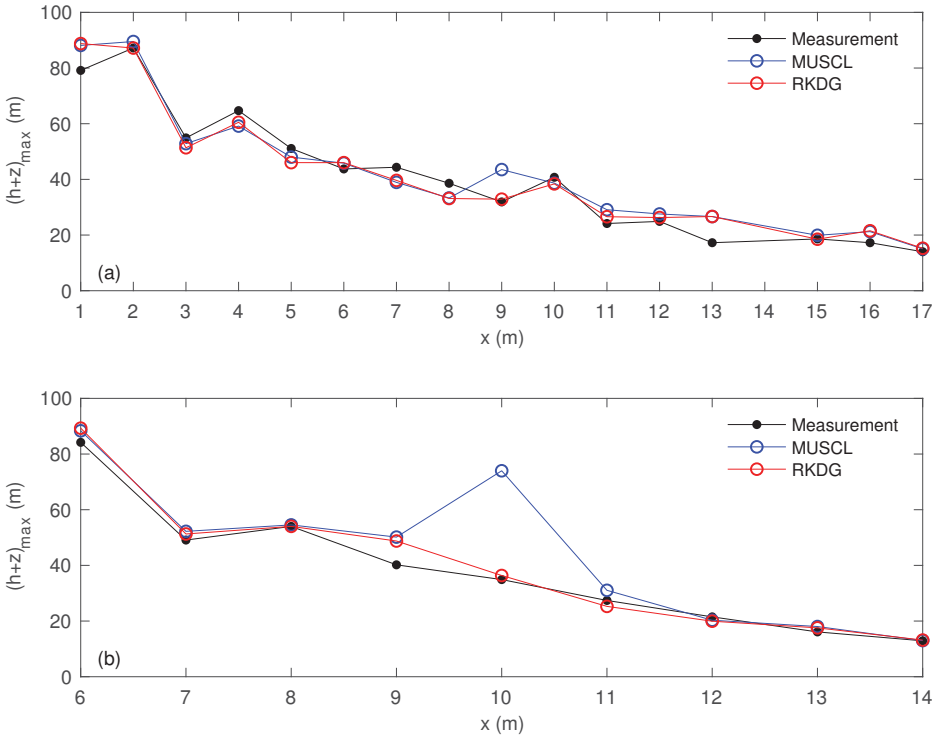

Fig. 9 Malpasset dam-break: comparison of numerical results (a) maximum water levels at survey points, (b) maximum water levels at experimental gauges

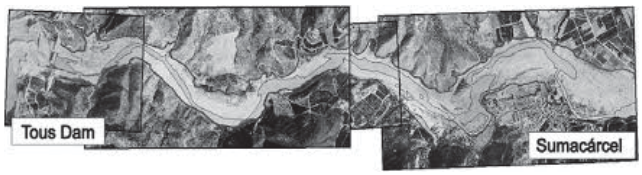

Fig. 10 Tous dam: Aerial view of the Júcar river reach from Tous dam to Sumacárcel about one week after the flood [57]

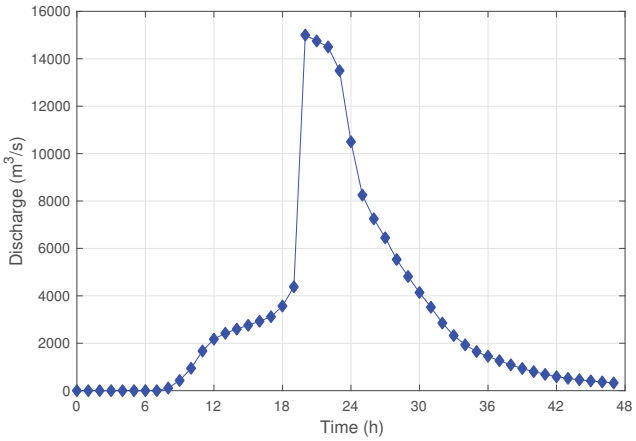

Fig. 11 Tous dam: discharge hydrograph imposed at the upstream boundary for the Tous dam

This work has therefore presented and compared two popular second-order numerical modelling alternatives for real-scale flood simulation: the MUSCL (non-local) spatial reconstruction approach and the local Discontinuous Galerkin (DG) approach. Both approaches have been taken with an explicit Runge-Kutta (RK) local time integration scheme, which were parallelized using the OpenMP platform. Simulations were conducted on a 24-core, dual socket 2.5 GHz Intel Xeon Haswell. Experimental and real-field benchmark tests are used to systematically compare between the models, focusing in particular on their response to mesh coarsening and parallel efficiency.

Comparisons between simulation results and reference data (i.e. analytical, experiments or field surveys) indicate that the two models generically lead to adequate performance. Consistent differences are detected in depth predictability and efficiency speedup relating to mesh coarsening and parallelisation. With coarsening of the mesh, results from the MUSCL calculations tend to deteriorate as compared with the RKDG ones, which remain better in the capture of water jumps, wave reflections and wet-dry front. Nonetheless, results among both models remain very close to each other at local zone where the flow is fluvial or gradual. In term of CPU runtime saving (on a single core), RKDG is undoubtedly more expensive on the same mesh due to its extra number of space operators, the need to apply the RK update to more-than-one coefficient at a time, and to the more restrictive CFL time step condition. However, considering further the superior accuracy of the RKDG outputs on the coarse mesh, the latter can be classified as more economical and practical; from the perspective that the mesh size that fits length-scale of the shallow wave features and/or topographic data are often not affordable/obtainable.

For the same test cases, the efficiency of the parallel implementation and its scaling effects have also been analysed considering also fine meshes (to more effectively exploit

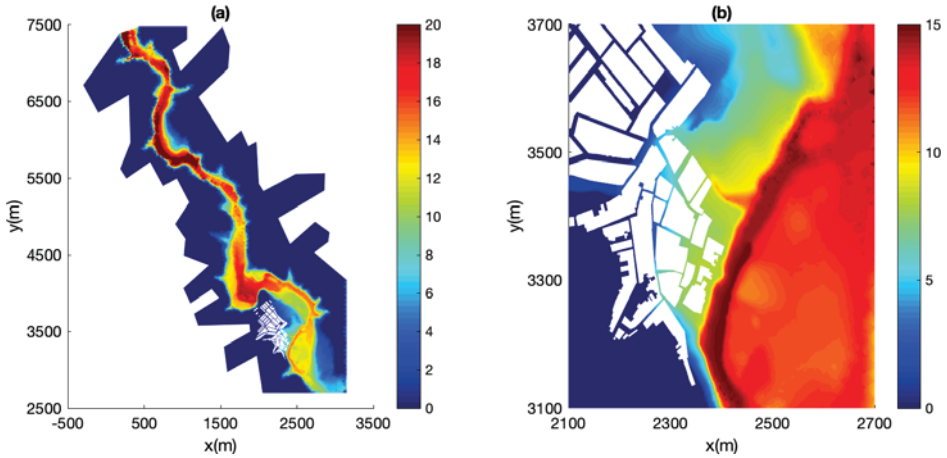

Fig. 12 Tous dam: computed maximum water depth by the RKDG model (a) in the whole valley, (b) in the town of Sumacárcel

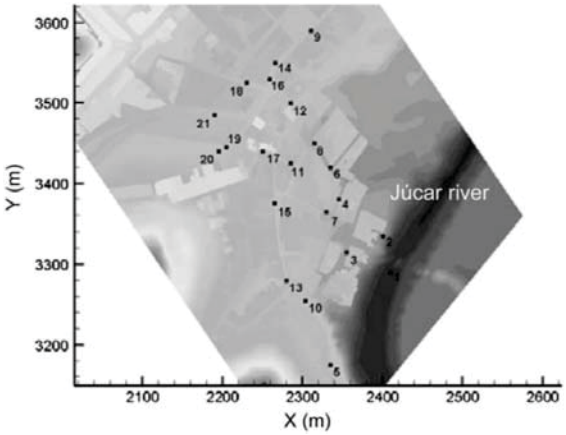

Fig. 13 Tous dam: locations of the gauges in the streets of Sumacárcel twon [57]

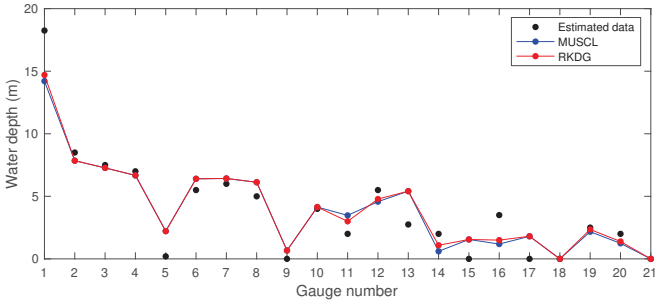

Fig. 14 Tous dam: measured and computed maximum water level at the different gauges

the power of parallelisation). The locality of the RKDG provides much better speedups than MUSCL, despite the RKDG overhead cost. The RKDG is found to be 10 to 12 % more efficient in term of parallel scalability, than MUSCL. Given further the above consideration, it can be concluded that parallel RKDG flood models are promising for use in real-scale application where domain geometry is often irregular and the fabric data is sparse.

REFERENCES

[1] J. Ernst, B. J. Dewals, S. Detrembleur, P. Archambeau, S. Erpicum, and M. Pirotton, "Micro-scale flood risk analysis based on detailed 2d hydraulic modelling and high resolution geographic data," *Nat. Hazards*, vol. 55, no. 2, pp. 181–209, 2010.

[2] L. Song, J. Zhou, J. Guo, Q. Zou, and Y. Liu, "A robust well-balanced finite volume model for shallow water flows with wetting and drying over irregular terrain," *Adv. Water Resour.*, vol. 34, no. 7, pp. 915–932, 2011.

[3] D. P. Viero, A. D?Alpaos, L. Carniello, and A. Defina, "Mathematical modeling of flooding due to river bank failure," *Adv. Water Resour.*, vol. 59, pp. 82–94, 2013.

[4] C. Dawson, C. J. Trahan, E. J. Kubatko, and J. J. Westerink, "A parallel local timestepping runge–kutta discontinuous Galerkin method with applications to coastal ocean modeling," *Comput. Methods Appl. Mech. Engrg.*, vol. 259, pp. 154–165, 2013.

[5] K. E. K. Abderrezzak, A. Paquier, and E. Mignot, "Modelling flash flood propagation in urban areas using a two-dimensional numerical model," *Nat. Hazards*, vol. 50, no. 3, pp. 433–460, 2009.

[6] Q. Liang, "Flood simulation using a well-balanced shallow flow model," *J. Hydraul. Eng.*, vol. 136, no. 9, pp. 669–675, 2010.

[7] G. Kesserwani and Y. Wang, "Discontinuous Galerkin flood model formulation: Luxury or necessity?" *Water Resources Res.*, vol. 50, no. 8, pp. 6522–6541, 2014.

[8] D. Sugawara and K. Goto, "Numerical modeling of the 2011 Tohoku-oki tsunami in the offshore and onshore of Sendai Plain, Japan," *Sediment. Geol.*, vol. 282, pp. 110–123, 2012.

[9] M. Akbar and S. Aliabadi, "Hybrid numerical methods to solve shallow water equations for hurricane induced storm surge modeling," *Environ. model. softw.*, vol. 46, pp. 118–128, 2013.

[10] K. Anastasiou and C. Chan, "Solution of the 2d shallow water equations using the finite volume method on unstructured triangular meshes," *Int. J. Numer. Methods Fluids*, vol. 24, no. 11, pp. 1225–1245, 1997.

[11] T. H. Yoon and S.-K. Kang, "Finite volume model for two-dimensional shallow water flows on unstructured grids," *J. Hydraul. Eng.*, vol. 130, no. 7, pp. 678–688, 2004.

[12] A. I. Delis, I. Nikolos, and M. Kazolea, "Performance and comparison of cell-centered and node-centered unstructured finite volume discretizations for shallow water free surface flows," *Arch. Comput. Methods Eng.*, vol. 18, no. 1, pp. 57–118, 2011.

[13] J. Murillo and P. García-Navarro, "Improved riemann solvers for complex transport in two-dimensional unsteady shallow flow," *J. Comput. Phys.*, vol. 230, no. 19, pp. 7202–7239, 2011.

[14] E. F. Toro, *Riemann solvers and numerical methods for fluid dynamics: a practical introduction, third ed.* Springer-Verlag, Berlin Heidelberg, 2009.

[15] B. F. Sanders, "Integration of a shallow water model with a local time step," *J. Hydraul. Res.*, vol. 46, no. 4, pp. 466–475, 2008.

[16] D. A. Haleem, G. Kesserwani, and D. Caviedes-Voullième, "Haar wavelet-based adaptive finite volume shallow water solver," *J. Hydroinform.*, vol. 17, no. 6, pp. 857–873, 2015.

[17] A. Lacasta, M. Morales-Hernández, J. Murillo, and P. García-Navarro, "Gpu implementation of the 2d shallow water equations for the simulation of rainfall/runoff events," *Environ. Earth Sci.*, vol. 74, no. 11, pp. 7295–7305, 2015.

[18] P. Brufau, M. Vázquez-Cendón, and P. García-Navarro, "A numerical model for the flooding and drying of irregular domains," *Int. J. Numer. Methods Fluids*, vol. 39, no. 3, pp. 247–275, 2002.

[19] I. Nikolos and A. Delis, "An unstructured node-centered finite volume scheme for shallow water flows with wet/dry fronts over complex topography," *Comput. Methods in Appl. Mech. Engrg.*, vol. 198, no. 47-48, pp. 3723–3750, 2009.

[20] Q. Liang and F. Marche, "Numerical resolution of well-balanced shallow water equations with complex source terms," *Adv. water Resour.*, vol. 32, no. 6, pp. 873–884, 2009.

[21] J. Hou, Q. Liang, F. Simons, and R. Hinkelmann, "A stable 2d unstructured shallow flow model for simulations of wetting and drying over rough terrains," *Comput. Fluids*, vol. 82, pp. 132–147, 2013.

[22] F. Aureli, A. Maranzoni, P. Mignosa, and C. Ziveri, "A weighted surface-depth gradient method for the numerical integration of the 2d shallow water equations with topography," *Adv. Water Resour.*, vol. 31, no. 7, pp. 962–974, 2008.

[23] F. Benkhaldoun, I. Elmahi, and M. Seaïd, "A new finite volume method for flux-gradient and source-term balancing in shallow water equations," *Comput. Methods Appl. Mech. Engrg.*, vol. 199, no. 49-52, pp. 3324–3335, 2010.

[24] Y. Wang, Q. Liang, G. Kesserwani, and J. W. Hall, "A 2d shallow flow model for practical dam-break simulations," *J. Hydraul. Res.*, vol. 49, no. 3, pp. 307–316, 2011.

[25] J. Hou, Q. Liang, F. Simons, and R. Hinkelmann, "A 2d well-balanced shallow flow model for unstructured grids with novel slope source term treatment," *Adv. Water Resour.*, vol. 52, pp. 107–131, 2013.

[26] J. Hou, Q. Liang, H. Zhang, and R. Hinkelmann, "An efficient unstructured muscl scheme for solving the 2d shallow water equations," *Environ. Modell. Softw.*, vol. 66, pp. 131–152, 2015.

[27] D. Schwanenberg and M. Harms, "Discontinuous Galerkin finite-element method for transcritical two-dimensional shallow water flows," *J. Hydraul. Eng.*, vol. 130, no. 5, pp. 412–421, 2004.

[28] J.-F. Remacle, S. S. Frazao, X. Li, and M. S. Shephard, "An adaptive discretization of shallow-water equations based on discontinuous Galerkin methods," *Int. J. Numer. Methods Fluids*, vol. 52, no. 8, pp. 903–923, 2006.

[29] A. Ern, S. Piperno, and K. Djadel, "A well-balanced runge–kutta discontinuous Galerkin method for the shallow-water equations with flooding and drying," *Int. J. Numer. Methods Fluids*, vol. 58, no. 1, pp. 1–25, 2008.

[30] G. Kesserwani, R. Ghostine, J. Vazquez, A. Ghenaim, and R. Mosé, "Application of a second-order Runge–Kutta discontinuous Galerkin scheme for the shallow water equations with source terms," *Int. J. Numer. Methods Fluids*, vol. 56, no. 7, pp. 805–821, 2008.

[31] S. Bunya, E. J. Kubatko, J. J. Westerink, and C. Dawson, "A wetting and drying treatment for the Runge–Kutta discontinuous Galerkin solution to the shallow water equations," *Comput. Methods Appl. Mech. Engrg.*, vol. 198, no. 17, pp. 1548–1562, 2009.

[32] R. Ghostine, G. Kesserwani, J. Vazquez, N. Rivière, A. Ghenaim, and R. Mose, "Simulation of supercritical flow in crossroads: Confrontation of a 2d and 3d numerical approaches to experimental results," *Comput. Fluids*, vol. 38, no. 2, pp. 425–432, 2009.

[33] G. Kesserwani and Q. Liang, "Locally limited and fully conserved rkdg2 shallow water solutions with wetting and drying," *J. Sci. Comput.*, vol. 50, no. 1, pp. 120–144, 2012.

[34] Y. Xing and X. Zhang, "Positivity-preserving well-balanced discontinuous Galerkin methods for the shallow water equations on unstructured triangular meshes," *J. Sci. Comput.*, vol. 57, no. 1, pp. 19–41, 2013.

[35] D. Wirasaet, E. Kubatko, C. Michoski, S. Tanaka, J. Westerink, and C. Dawson, "Discontinuous Galerkin methods with nodal and hybrid modal/nodal triangular, quadrilateral, and polygonal elements for nonlinear shallow water flow," *Comput. Methods Appl. Mech. engrg.*, vol. 270, pp. 113–149, 2014.

[36] N. Wintermeyer, A. R. Winters, G. J. Gassner, and D. A. Kopriva, "An entropy stable nodal discontinuous Galerkin method for the two dimensional shallow water equations on unstructured curvilinear meshes with discontinuous bathymetry," *J. Comput. Phys.*, vol. 340, pp. 200–242, 2017.

[37] G. Kesserwani, J. L. Ayog, and D. Bau, "Discontinuous Galerkin formulation for 2d hydrodynamic modelling: Trade-offs between theoretical complexity and practical convenience," *Comput. Methods Appl. Mech. Engrg.*, vol. 342, pp. 710–741, 2018.

[38] G. Kesserwani and Q. Liang, "A discontinuous Galerkin algorithm for the two-dimensional shallow water equations," *Comput. Methods Appl. Mech. Engrg.*, vol. 199, no. 49-52, pp. 3356–3368, 2010.

[39] D. Caviedes-Voullième and G. Kesserwani, "Benchmarking a multiresolution discontinuous Galerkin shallow water model: Implications for computational hydraulics," *Adv. Water Resour.*, vol. 86, pp. 14–31, 2015.

[40] B. Cockburn, S. Hou, and C.-W. Shu, "The Runge–Kutta local projection discontinuous Galerkin finite element method for conservation laws. IV. The multidimensional case," *Math. Comput.*, vol. 54, no. 190, pp. 545–581, 1990.

[41] C. Dawson and J. Proft, "Discontinuous and coupled continuous/discontinuous Galerkin methods for the shallow water equations," *Comput. Methods Appl. Mech. Engrg.*, vol. 191, no. 41, pp. 4721–4746, 2002.

[42] C. Eskilsson, "An hp-adaptive discontinuous Galerkin method for shallow water flows," *Int. J. Numer. Methods Fluids*, vol. 67, no. 11, pp. 1605–1623, 2011.

[43] B. Kim, B. F. Sanders, J. E. Schubert, and J. S. Famiglietti, "Mesh type tradeoffs in 2d hydrodynamic modeling of flooding with a Godunov-based flow solver," *Adv. Water Resour.*, vol. 68, pp. 42–61, 2014.

[44] E. Mignot, A. Paquier, and S. Haider, "Modeling floods in a dense urban area using 2D shallow water equations," *J. Hydrol.*, vol. 327, no. 1, pp. 186–199, 2006.

[45] J. E. Schubert and B. F. Sanders, "Building treatments for urban flood inundation models and implications for predictive skill and modeling efficiency," *Adv. Water Resour.*, vol. 41, pp. 49–64, 2012.

[46] M. V. Bilskie and S. C. Hagen, "Topographic accuracy assessment of bare earth lidar-derived unstructured meshes," *Adv. Water Resour.*, vol. 52, pp. 165–177, 2013.

[47] M. Hubbard, "Multidimensional slope limiters for MUSCL-type finite volume schemes on unstructured grids," *J. Comput. Phys.*, vol. 155, no. 1, pp. 54–74, 1999.

[48] Y. Xing and C.-W. Shu, "A new approach of high order well-balanced finite volume WENO schemes and discontinuous Galerkin methods for a class of hyperbolic systems with source terms," *Commun. Comput. Phys.*, vol. 1, no. 1, pp. 100–134, 2006.

[49] L. Begnudelli, B. F. Sanders, and S. F. Bradford, "Adaptive Godunov-based model for flood simulation," *J. Hydraul. Eng.*, vol. 134, no. 6, pp. 714–725, 2008.

[50] B. Cockburn and C.-W. Shu, "The Runge–Kutta discontinuous Galerkin method for conservation laws V: multidimensional systems," *J. Comput. Phys.*, vol. 141, no. 2, pp. 199–224, 1998.

[51] W. Thaker, "Some exact solutions to the nonlinear shallow-water equations," *J. Fluid Mech.*, vol. 107, pp. 499–508, 1981.

[52] M. Sun and K. Takayama, "Error localization in solution-adaptive grid methods," *J. Comput. Phys.*, vol. 190, no. 1, pp. 346–350, 2003.

[53] G. Testa, D. Zuccalà, F. Alcrudo, J. Mulet, and S. Soares-Frazão, "Flash flood flow experiment in a simplified urban district," *J. Hydraul. Res.*, vol. 45, no. sup1, pp. 37–44, 2007.

[54] N. Goutal, "The Malpasset dam failure. An overview and test case definition," in *Proc. of the 4th CADAM meeting*, Zaragoza, Spain, 1999.

[55] A. Valiani, V. Caleffi, and A. Zanni, "Case study: Malpasset dam-break simulation using a two-dimensional finite volume method," *J. Hydraul. Eng.*, vol. 128, no. 5, pp. 460–472, 2002.

[56] P. Brufau, P. García-Navarro, and M. Vázquez-Cendón, "Zero mass error using unsteady wetting–drying conditions in shallow flows over dry irregular topography," *Int. J. Numer. Methods Fluids*, vol. 45, no. 10, pp. 1047–1082, 2004.

[57] F. Alcrudo and J. Mulet, "Description of the Tous dam break case study (Spain)," *J. Hydraul. Res.*, vol. 45, no. sup1, pp. 45–57, 2007.

[58] E. Mignot and A. Paquier, "Impact flood propagation case study: The flooding of Sumacárcel after Tous dam break, Cemagref modelling," in *Proc. of the 4th Impact Project Workshop*, Zaragoza, Spain, 2004.

[59] J. Mulet and F. Alcrudo, "Impact flood propagation case study: The flooding of Sumacárcel after Tous dam break, University of Zaragoza modelling," in *Proc. of the 4th Impact Project Workshop*, Zaragoza, Spain, 2004.

[60] S. Soares Frazao and Y. Zech, "The Tous dam break: Description of the simulations performed at UCL," in *Proc. of the 4th Impact Project Workshop*, Zaragoza, Spain, 2004.

[61] J. Mulet and F. Alcrudo, "Uncertainty analysis of Tous flood propagation case study," in *Proc. of the 4rd Impact Project Workshop*, Zaragoza, Spain, 2004.